IEEE Access
Multidisciplinary | Rapid Review | Open Access Journal

Received April 15, 2019, accepted July 17, 2019, date of publication July 22, 2019, date of current version August 2, 2019.

Digital Object Identifier 10.1109/ACCESS.2019.2930301

Performance Evaluation of a Hollowed Multi-Drum Magnetorheological Brake Based on Finite Element Analysis Considering Hollow Casing Radius

HUANHUAN QIN, (Student Member, IEEE), AIGUO SONG, (Senior Member, IEEE), AND YITING MO

The State Key Laboratory of Bioelectronics, Southeast University, Nanjing 210096, China
Jiangsu Key Lab of Remote Measurement and Control, School of Instrument Science and Engineering, Southeast University, Nanjing 210096, China

Corresponding author: Aiguo Song (a.g.song@seu.edu.cn)

This work was supported in part by the National Key Research and Development Program of China under Grant 2016YFB1001301, and in part by the Natural Science Foundation of China under Grant U1713210 and Grant 91648206.

ABSTRACT Based on the rheological effect of magnetorheological (MR) fluid, MR brake is a promising actuator due to its passiveness, high torque density, and low power consumption. This paper focuses on a unique hollowed multi-drum MR brake which has a hollow casing and several drum-like rotors and stators and evaluates the influence of the hollow casing radius on the performance of this brake. First, the brakes with different hollow casing radii were optimized via finite element analysis to obtain the optimal designs. Then, the torque, volume, mass, and power consumption including torque volume, torque mass, and torque power ratios were calculated to conduct the performance evaluation. According to the results, the suggestion on the hollow casing radius was given in the hollowed multi-drum brake design. To validate finite element analysis, the brake with 8-mm hollow casing radius was fabricated, assembled, and tested. The test results were generally consistent with the results of finite element analysis.

INDEX TERMS Hollowed multi-drum MR brake, hollow casing radius, finite element analysis, performance evaluation.

I. INTRODUCTION

MR fluid, which is a suspension of miniature ferromagnetic particles and the carrier fluid, is a new type of intelligent engineering material [1]. It has the rheological effect, that is, under the application of an external magnetic field, the ferromagnetic particles can form a chain-like structure, so that it turns to the semi-solid state. After removing the magnetic field, it restores to the liquid state again. During this period, the yield stress of MR fluid can be reversely and continuously changed according to the intensity of the magnetic field. MR brake is a promising actuator based on the rheological effect of MR fluid. Due to its characteristics of passiveness, high torque density, and low power consumption, MR brakes have been widely used in the fields of force feedback devices [2], [3], rehabilitation robots [4], [5] and automotive industry [6], [7].

Recently, researchers have conducted extensive studies on the optimization and performance evaluation of MR brake using finite element analysis (FEA). Nguyen and Choi presented an optimization of a disk-type MR brake for automotive applications [8]. FEA was used to obtain the optimal design parameters taking the torque output, mass, and dimensions of the brake and the temperature due to the zero-field friction of the MR fluid into consideration. Based on the FEA results, the most suitable MR brake design for the middle-sized passenger car was obtained. Gao and Liao evaluated the influence of the position of the inner coil on the performance of a multi-disk MR brake [9]. Brakes with the interior, exterior, and axial inner coils were considered and compared. The comparison results showed that the interior inner coil was the best configuration in terms of torque output. Then, the

The associate editor coordinating the review of this manuscript and approving it for publication was Yangmin Li.

brake with the interior inner coil was optimized and FEA was used to verify the optimized design. Nguyen and Choi presented an optimal selection among disk-type, drum-type, hybrid-type, and T-shaped type MR brakes mainly considering the maximum torque and given volume [10]. To conduct a fair comparison, each brake was optimized via FEA. The optimization goals were to maximize the torque output within a specified cylindrical volume while the torque ratio should be larger than the given value. Li et al. conducted a performance comparison among three different configurations: drum, single-disk, and multi-disk types [11]. Similarly, in order to obtain fair results, the three configurations were optimized using FEA. Then, the characteristics in terms of the geometrical dimensions, mass, torque output, and power consumption were calculated and compared. Ma et al. designed and optimized a multi-disk MR brake with an interior inner coil for rehabilitation device [12]. A modified internal structure was proposed to maximize the magnetic flux. FEA was adopted to obtain the optimal geometrical internal structure. Patil et al. presented the thermal analysis of a disk-type MR brake to predict the temperature performance under braking maneuver [13]. FEA was used to observe the temperature distribution within the brake under the transient effects and the drive cycle. FEA results showed that there were rises of about 10 °C and 0.5 °C, respectively, which were consistent with the experimental results. Yu et al. proposed an optimal methodology to improve the performance of a T-shaped MR brake under various temperature [14]. FEA was integrated into the optimization process. In FEA, the non-dominated sorting genetic algorithm II was utilized to solve the multi-objective equations. The maximum braking torque, dynamic range, and mass of the brake were configured as the design objectives. Shamieh and Sedaghati designed a two-disk MR brake with no zero-field viscous torque [15]. FEA was used to obtain the optimal design parameters. In FEA, the genetic algorithm and the sequential quadratic programming algorithm were integrated. The optimization problem was to maximize the torque output while minimizing the response time and mass of the MR brake.

In the above literature, disk-type and drum-type MR brakes have been sufficiently discussed. This paper focuses on a unique hollowed multi-drum MR brake which has a hollow casing and several drum-like rotors and stators. This type of MR brake can be used not only as a passive actuator with higher torque density but also to construct a compact hybrid actuator with other actuation methods (such as DC motor). In the design of a hollowed multi-drum brake, the hollow casing radius is an important parameter since it has a significant influence on the brake performance. Therefore, the performance evaluation of the hollowed multi-drum brake considering the hollow casing radius is conducted in this paper. The brakes with different hollow casing radii were optimized to obtain the optimal designs using FEA. Then, the torque, volume, mass, and power consumption including torque-volume, torque-mass, and torque-power ratios (TVR, TMR, and TPR) were calculated and evaluated.

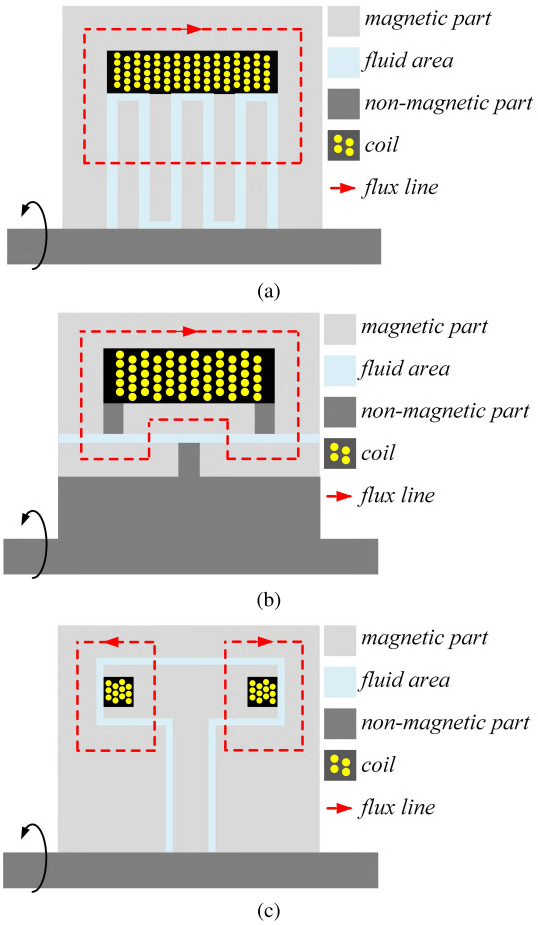

FIGURE 1. Typical MR brake structures. (a) Disk-type brake, (b) drum-type brake, and (C) T-shaped type brake.

According to the results of the evaluation, the suggestion on the hollow casing radius was given. To verify the FEA results, the brake with 8 mm hollow casing radius was fabricated, assembled, and tested.

II. HOLLOWED MULTI-DRUM MR BRAKE STRUCTURE

According to the structures, MR brakes can be mainly categorized into: disk-type brakes [16], [17], drum-type brakes [18], [19], and T-shaped type brakes [20], [21] (shown in FIGURE 1). Disk-type brake has one or several disk-like rotors and stators. This type of MR brake can balance structural simplicity and compactness. Drum-type brake usually has a cylindrical rotor and is characterized by large inertia. The serpentine flux path and the inverted-drum structure are two techniques commonly used in drum-type brake designs. T-shaped type brake usually has a T-flange structure and two coils. The outer and inner surfaces of the T-flange can become active shearing areas. Different from the structures above, the hollowed multi-drum structure discussed in this paper has a hollow casing and several drum-like rotors and stators. The hollow casing is convenient to insert other actuators, such as DC motor, into the brake. The drum-like rotors and stators can activate more shearing areas within a limited volume. Therefore, this type of brake can be used not only as a passive

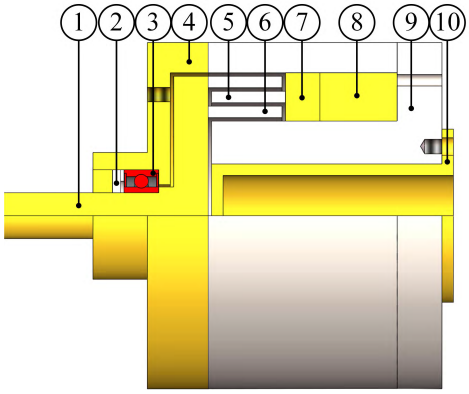

FIGURE 2. Hollowed multi-drum brake structure. (1) Shaft, (2) magnetic ring, (3) sealed bearing, (4) non-magnetic front casing, (5) stator, (6) rotor, (7) stator holder, (8) coil, (9) magnetic rear casing, and (10) non-magnetic inner casing.

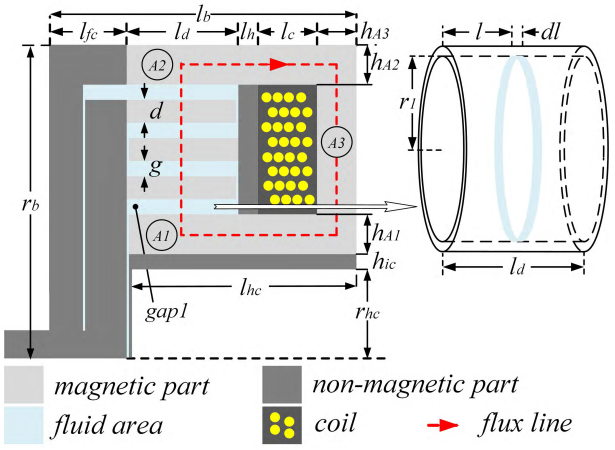

FIGURE 3. Simplified and parametric model of hollowed multi-drum brake.

actuator with higher torque density but also to construct a compact hybrid actuator with other actuation methods. The general structure of the hollowed multi-drum brake is shown in FIGURE 2. To facilitate analysis, the triple-drum structure is taken as an example in this paper. The following FEA simulation and performance evaluation are based on this triple-drum structure.

In this structure, a sealed bearing is utilized to support the shaft. A magnetic ring is utilized for MR fluid leakage prevention. Compared with conventional methods [22]–[24], this method can reduce the off-state torque due to mechanical friction while having a good sealing effect. Two gaps are formed between three drums (two rotors and one stator). Two more gaps are formed between the rotors and the magnetic rear casing. These gaps will be filled with MR fluid when fully injected. The rotors are connected to the shaft and rotate synchronously with the shaft. The stator is connected to the stator holder and keeps fixed with the brake casing. The coil, which is wound using enameled copper wire, is placed against the stator holder to generate a magnetic field over fluid gaps. The non-magnetic inner casing, which is connected to the magnetic rear casing, reserves enough space for other actuators.

III. OPTIMIZATION AND PERFORMANCE EVALUATION

The simplified and parametric model of the hollowed multi-drum brake is illustrated in FIGURE 3. To simplify the analysis, the magnetic rear casing is split into three parts: areas $A1$, $A2$, and $A3$. r_{hc} represents the hollow casing radius.

A. MR BRAKE MODEL

1) BRAKING TORQUE

In this paper, the Bingham model is used to describe the rheological behavior of MR fluid, which can be expressed as:

$$\tau = \tau_y(H) + \eta\dot{\gamma}, \quad \tau > \tau_y(H) \tag{1}$$

where H and $\tau_y(H)$ represent the magnetic field strength and the field-dependent yield stress, respectively. η and $\dot{\gamma}$ represent the viscous friction coefficient and the shear rate, respectively.

Generally, the torque output T of an MR brake is composed of two parts: the field-dependent torque and the viscous torque. Due to the low angular velocity of the brake in this paper, the viscous torque is neglected. Hence, T over the shear area A can be calculated as:

$$T = \int_A r\tau_y(H)dA \tag{2}$$

where r is the radius of the shear area.

The brake has four fluid gaps. Taking the smallest gap (the gap1 in FIGURE 3) as an example, the torque output of this gap can be written as:

$$\begin{aligned} T_1 = \int_{A_1} r_1\tau_y(H_1)dA_1 &= \int_0^{l_d} r_1\tau_y(H_1)\cdot 2\pi r_1 dl \\ &= 2\pi {r_1}^2 l_d \tau_y(H_1) \end{aligned} \tag{3}$$

where r_1 is selected as the inner radius of gap1. There would be no significant influence on T if the radius here is selected as the outer radius or the average of the inner and outer radii since the fluid gap is small. l_d represents the length of the drum.

Therefore, the total torque output generated over four gaps can be calculated as:

$$T = \sum_{i=1}^{4} T_i = \sum_{i=1}^{4} 2\pi {r_i}^2 l_d \tau_y(H_i) \tag{4}$$

where r_i is the inner radius of each gap. It can be expressed as:

$$r_i = r_{hc} + h_{ic} + h_{A1} + (i-1)d + (i-1)g \tag{5}$$

where r_{hc} is the hollow casing radius. h_{ic} is the thickness of the non-magnetic inner casing. h_{A1} is the thickness of the magnetic rear casing area $A1$. d and g represent the thickness of the drum and the fluid gap, respectively.

In this brake, the MR fluid is selected as MRF-122EG from LORD Corporation. In actual torque calculation, the flux

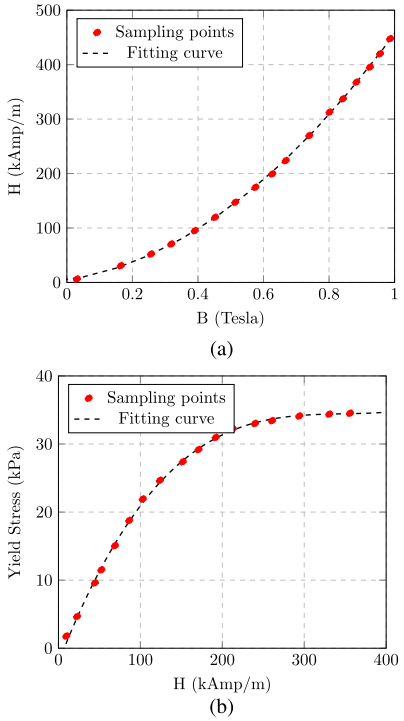

FIGURE 4. MRF-122EG technical data. (a) Relationship between magnetic field strength and flux density. (b) Relationship between yield stress and magnetic field strength.

density data is obtained from FEA simulation at first. According to the MRF-122EG data (shown in FIGURE 4), the magnetic field strength and the fluid yield stress can be calculated. Then, the torque output of the brake can be obtained.

2) VOLUME

The volume can be roughly expressed as:

$$V = \pi(r_b^2 l_b - r_{hc}^2 l_{hc}) \tag{6}$$

where r_b and l_b represent the radius and length of the brake, respectively. r_{hc} and l_{hc} represent the radius and length of the hollow casing, respectively.

r_b, l_b, and l_{hc} can be roughly expressed as:

$$\begin{cases} r_b = r_{hc} + h_{ic} + h_{A1} + 3d + 4g + h_{A2} \\ l_b = l_{fc} + l_d + l_h + l_c + h_{A3} \\ l_{hc} = l_d + l_h + l_c + h_{A3} \end{cases} \tag{7}$$

where h_{A2} and h_{A3} represent the thickness of the magnetic rear casing areas $A2$ and $A3$, respectively. l_{fc}, l_h, and l_c represent the length of the non-magnetic front casing, stator holder, and coil, respectively.

Combining equations 6 and 7, the volume of the brake can be calculated.

3) MASS

The total mass of the brake can be treated as the sum of the mass of each material. In this brake, the non-magnetic material is selected as copper. The magnetic material is selected as electric pure iron (DT4C). Hence, the mass of the brake can be expressed as:

$$M = V_{Cu}\rho_{Cu} + V_{DT4}\rho_{DT4} + V_{MR}\rho_{MR} \tag{8}$$

where V and ρ represent volume and density of each material, respectively. According to the technical data, $\rho_{Cu} = 8.50$ g/cm^3, $\rho_{DT4} = 7.87$ g/cm^3, and $\rho_{MR} = 2.38$ g/cm^3. The volume of each material can be roughly expressed as:

$$\begin{aligned} V_{Cu} = {} & \pi r_b^2 l_{fc} + \pi[(r_{hc} + h_{ic})^2 - r_{hc}^2] l_{hc} \\ & + \pi[(r_b - h_{A2})^2 - (r_{hc} + h_{ic} + h_{A1})^2](l_h + l_c) \end{aligned} \tag{9}$$

$$\begin{aligned} V_{DT4} = {} & \pi[r_b^2 - (r_b - h_{A2})^2] l_{hc} \\ & + \pi[(r_{hc} + h_{ic} + h_{A1})^2 - (r_{hc} + h_{ic})^2] l_{hc} \\ & + \pi[(r_b - h_{A2})^2 - (r_{hc} + h_{ic} + h_{A1})^2] h_{A3} \\ & + \sum_{i=1}^{3} \pi[(r_i + g + d)^2 - (r_i + g)^2] l_d \end{aligned} \tag{10}$$

$$V_{MR} = \sum_{i=1}^{4} \pi[(r_i + g)^2 - r_i^2] l_d \tag{11}$$

Combining equations 8, 9, 10, and 11, the mass of the brake can be obtained.

4) POWER CONSUMPTION

The power consumption of the brake can be expressed as:

$$P = I^2 R_c \tag{12}$$

where R_c is the resistance of the coil, which can be written as:

$$R_c = L_w R_w = N_c \pi D_{cavg} R_w \tag{13}$$

where L_w and R_w represent the total length of the wire and the resistance per unit length of the wire, respectively. N_c is the number of coil turns. D_{cavg} is the average diameter of the coil, which can be expressed as: $D_{cavg} = 2r_{hc} + 2h_{ic} + 2h_{A1} + 3d + 4g$.

The number of coil turns can be calculated as:

$$N_c = \frac{(3d + 4g) l_c}{d_w^2} \eta \tag{14}$$

where d_w and η represent the diameter of the wire and the winding efficiency, respectively. In this brake, the wire is selected as the 0.25 mm diameter enameled copper wire, then, $R_w = 0.3345$ Ω/m. η is selected to be 65%.

B. OPTIMIZATION BASED ON FEA

For a fair comparison, the brakes with different hollow casing radii (r_{hc}) were optimized using FEA. The optimization started with 4 mm hollow casing radius. The radius increased with a step of 4 mm until it reached 20 mm. Then, the radius increased with a step of 10 mm until it reached the maximum value. In order to show as clearly as possible the influence of the hollow casing radius on the brake performance, the maximum value was selected to be 250 mm, although the radius

TABLE 1. MR brake active variables.

Variable	Description	Range
h_{A1}	thickness of magnetic area $A1$	3 - 5 mm
h_{A2}	thickness of magnetic area $A2$	2 - 4 mm
h_{A3}	thickness of magnetic area $A3$	3 - 5 mm
$\mathscr{F}$	magnetomotive force	200 - 350 AT*

* AT represents ampere-turns.

TABLE 2. MR brake constant variables.

Variable	Description	Value (mm)
l_{fc}	length of front casing	5
l_d	length of drum	6
l_h	length of stator holder	3
l_c	length of coil	7
d	thickness of drum	1
g	thickness of gap	0.3
h_{ic}	thickness of inner casing	1

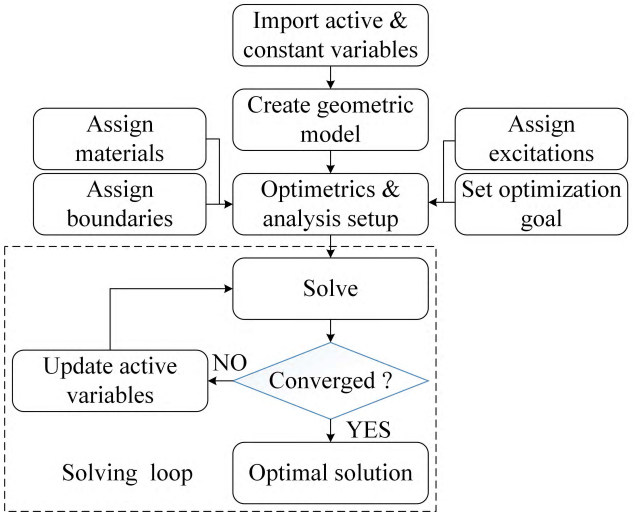

FIGURE 5. Optimization process under given hollow casing radius.

would not reach this value in most applications. The additional 10 mm hollow casing radius was also included in the optimization. In order to facilitate the optimization, based on the influence on the performance evaluation, the four parameters were selected as active variables (shown in TABLE 1) to indicate the optimal design and other parameters were configured as constant variables (shown in TABLE 2). Before the formal optimization, two experimental simulations under the minimum and maximum hollow casing radii were conducted to predict the ranges of the active variables. Considering the results of the experimental simulations, the ranges of the active variables were also given in TABLE 1.

The general optimization process under a given hollow casing radius is shown in FIGURE 5. At first, the initial active and constant variables were imported into ANSYS software to create the geometric model. After the optimetrics and analysis setup (e.g. material, excitation, and boundary assignment), the pattern search algorithm was started to find the optimal active variables. In the optimization, the goal was

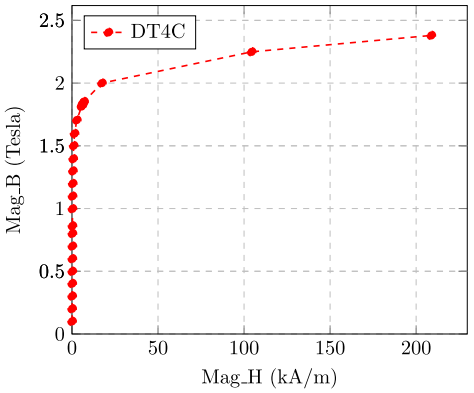

FIGURE 6. B-H data of DT4C.

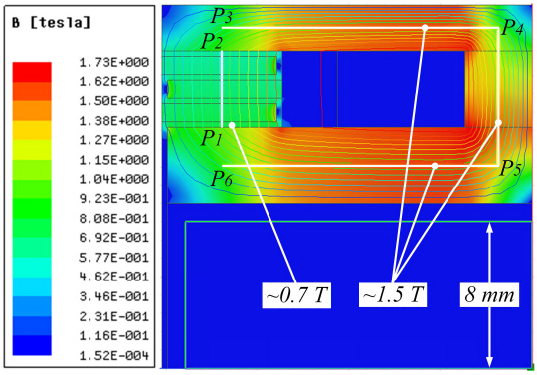

FIGURE 7. FEA results under 8 mm hollow casing radius.

to ensure that the flux density over the smallest gap (gap1) was around the MRF-122EG saturation point (0.7 T) and the maximal flux density along the iron flux path was around the DT4C saturation point (1.5 T) [25]. After obtaining all the optimal designs, the torque, volume, mass, and power consumption including TVR, TMR, and TPR were calculated and evaluated. In the material assignment, the relative permeability of MRF-122EG and DT4C was set to non-linear, and the B-H data of the two materials (shown in FIGURE 4a and FIGURE 6) was imported. The relative permeability of copper was set to 0.999991.

C. RESULTS AND DISCUSSION

Taking 8 mm hollow casing radius as an example, the FEA simulation results are shown in FIGURE 7. Generally, the flux density over the smallest gap reached around 0.7 T and the maximal flux density along the iron path reached around 1.5 T.

In order to specifically demonstrate the FEA simulation, the flux density distribution under 8 mm hollow casing radius was detected. The flux density detection over the gaps started from P_1 to P_2. The flux density along the iron path was individually detected between P_3 and P_4, between P_4 and P_5, and between P_5 and P_6 (shown in FIGURE 7). As shown in FIGURE 8 and FIGURE 9, the average flux density over the smallest gap was detected as 695.30 mT and the maximal flux density in magnetic areas $A1$, $A2$, and $A3$ were 1.52, 1.50, and 1.49 T, respectively. These indicated that both MRF-122EG

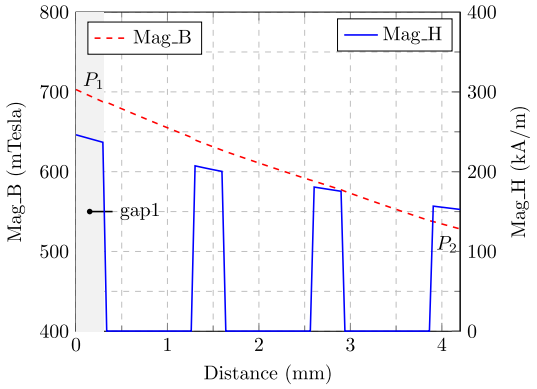

FIGURE 8. Magnetic flux density and field strength over fluid gaps under 8 mm hollow casing radius.

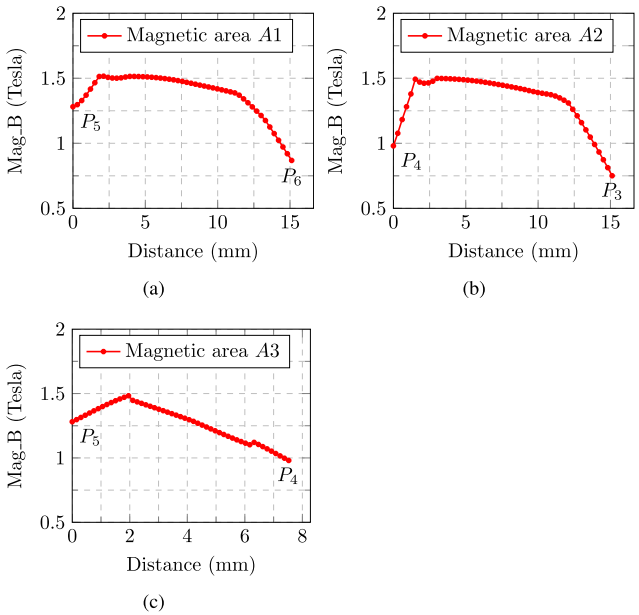

FIGURE 9. Magnetic flux density along iron path under 8 mm hollow casing radius. (a) Magnetic area *A*1, (b) magnetic area *A*2, and (c) magnetic area *A*3.

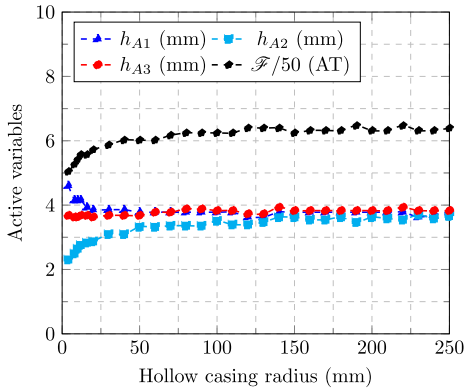

FIGURE 10. Optimal active variables under each hollow casing radius.

and DT4C reached their saturation points under the same excitation.

The final optimal active variables under each hollow casing radius are shown in FIGURE 10. Generally, with the increase

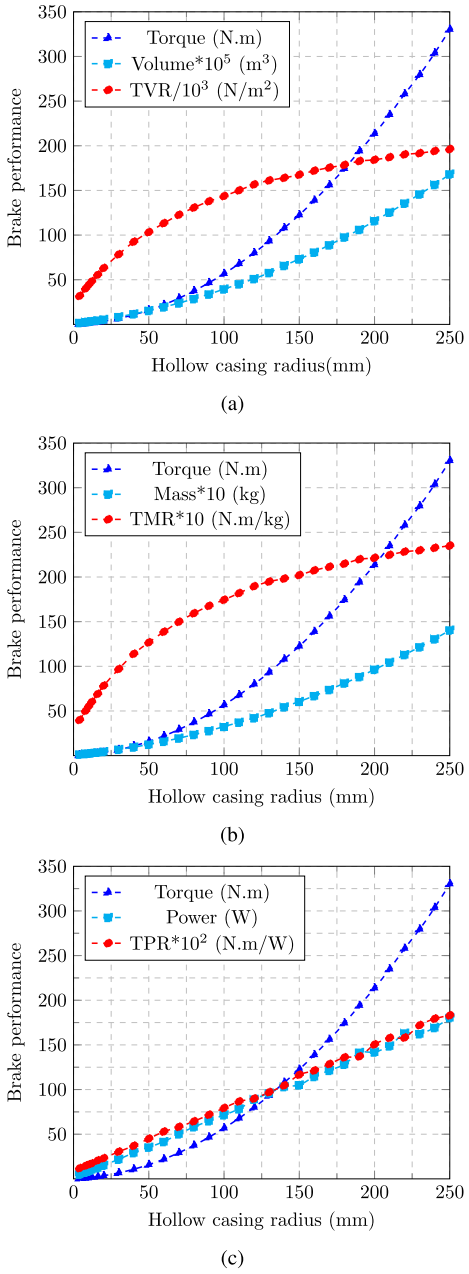

FIGURE 11. Brake performance. (a) Torque, volume, and TVR, (b) torque, mass, and TMR, and (c) torque, power consumption, and TPR.

of the hollow casing radius, h_{A2} and $\mathscr{F}$ showed an upward trend while h_{A1} showing a downward trend. After about 100 mm radius, both trends were limited. h_{A3} showed a slight fluctuation with the increase of the hollow casing radius.

The performance was calculated in FIGURE 11. When the hollow casing radius was increased from 4 to 250 mm, the torque showed a significant increase from 0.61 to 330.18 N.m. The volume also increased significantly from $1.92*10^{-5}$ to $168.27*10^{-5}$ m^3. Due to the greater increase in torque than in volume, there was also an increase in TVR (shown in FIGURE 11a). The TVR increased steadily from $31.89*10^3$ to $196.22*10^3$ N/m^2. Similarly, the mass and TMR (shown in FIGURE 11b)

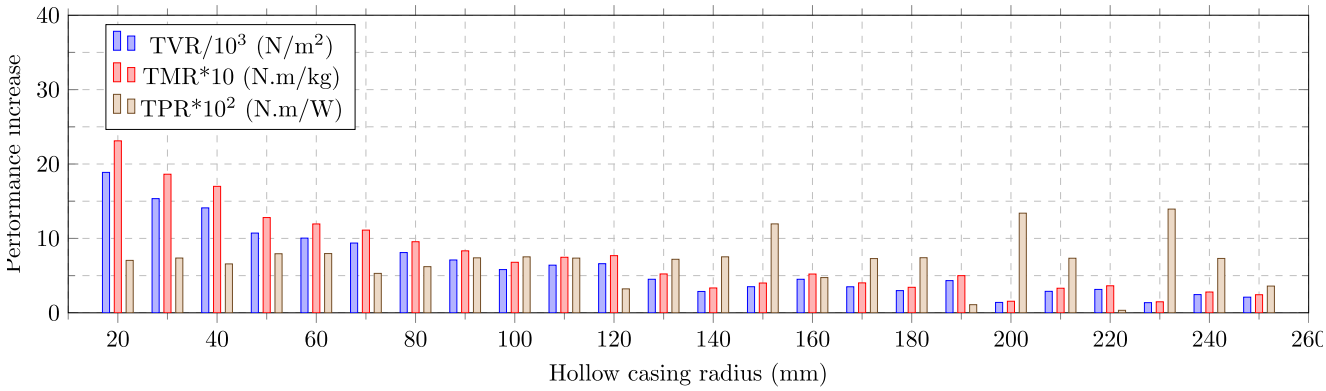

FIGURE 12. Performance increase per 10 mm radius step.

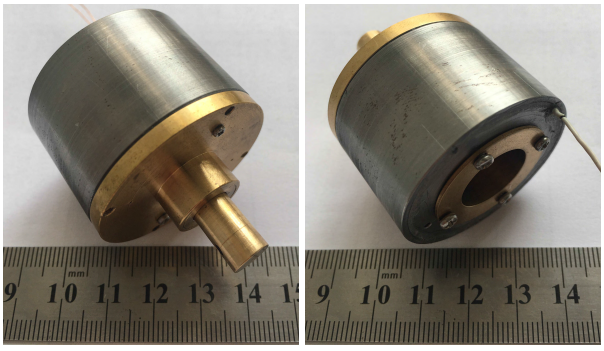

(a) (b)

FIGURE 13. Fabricated hollowed multi-drum brake with 8 mm hollow casing radius. (a) Front view and (b) rear view.

increased from $1.53*10^{-1}$ to $140.47*10^{-1}$ kg and from $39.99*10^{-1}$ to $235.05*10^{-1}$ N.m/kg, respectively. The power consumption and TPR (shown in FIGURE 11c) almost had a linear increase with the increase of the hollow casing radius, from 5.12 to 180.42 W and from $11.96*10^{-2}$ to $183.01*10^{-2}$ N.m/W, respectively.

The performance increase per 10 mm radius step is shown in FIGURE 12. The performance increase under 20 mm radius was calculated as the difference between 10 and 20 mm radii. The same calculation principle applied to the other radii. It can be observed from the figure that the increase of both TVR and TMR showed a downward trend with the increase of the hollow casing radius. When the radius increased from 10 to 20 mm, there was an $18.87*10^3$ N/m^2 increase in TVR and a $23.11*10^{-1}$ N.m/kg increase in TMR. However, when the radius increased from 140 to 150 mm, the increase of TVR was only $3.51*10^3$ N/m^2 and the increase of TMR was only $4.0*10^{-1}$ N.m/kg. Finally, when the radius increased from 240 to 250 mm, the increase of TVR and TMR were $2.10*10^3$ N/m^2 and $2.43*10^{-1}$ N.m/kg, respectively. This trend was not observed in TPR.

Generally, the brake performance in terms of TVR, TMR, and TPR improved with the increase of the hollow casing radius. From this point, the hollow casing radius should be kept as large as possible within the design range in the hollowed multi-drum MR brake design. However, the designers should pay attention to the increase of TVR and TMR. After about 100 mm radius, the increasing trends of both TVR and TMR were limited.

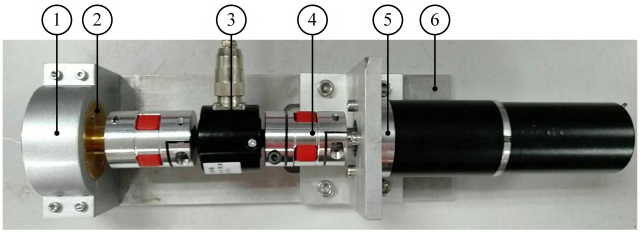

FIGURE 14. Torque test setup. (1) Brake holder, (2) MR brake, (3) torque sensor, (4) coupling, (5) Maxon motor, and (6) base.

TABLE 3. FEA and actual test results of MR brake.

Items	FEA values	Actual values
Torque (N.m)	1.07	$\sim$ 1.08
Volume (m^3)	$2.67*10^{-5}$	$2.67*10^{-5}$
TVR (N/m^2)	$40.13*10^3$	$40.45*10^3$
Mass (kg)	$2.14*10^{-1}$	$2.32*10^{-1}$
TMR (N.m/kg)	$50.17*10^{-1}$	$46.55*10^{-1}$
Power consumption (W)	7.28	8.00
TPR (N.m/W)	$14.75*10^{-2}$	$13.50*10^{-2}$

IV. FEA VALIDATION

To validate FEA, a brake with 8 mm hollow casing radius (shown in FIGURE 13) was fabricated, assembled and tested. This brake was convenient to construct a compact hybrid actuator with the micromotor (1524012SR, Faulhaber).

The h_{A1}, h_{A2}, and h_{A3} in fabrication were 4.10, 2.50, and 3.60 mm, respectively. The brake had 39.5 mm outer diameter and 25 mm length. It weighed about 232 g. The power consumption of the brake was about 8.0 W. The torque was measured using the setup in FIGURE 14. The Maxon motor combination (RE40, Maxon) was used to rotate the brake in one direction at 30 r/min. The brake was fixed to the base via the brake holder. The braking torque was recorded using a torque sensor (SY8414, ShuYi Corporation). The FEA simulation showed that the brake under 8 mm hollow casing radius would reach its saturation torque at around 860 mA.

TABLE 4. Performance comparisons among small-scale MR brakes.

	Current work	MR brake [3]	MR brake [25]	MR brake[a] [2]
Architecture	Hollowed multi-drum	Multi-disk	Multi-drum	Drum
Torque (N.m)	$\sim 1.08^{b}$	0.48	0.403	0.399
Volume (m^3)	$2.67*10^{-5}$	$1.83*10^{-5}$	$1.45*10^{-5}$	$1.05*10^{-5}$
TVR (N/m^2)	$40.45*10^{3}$	$26.21*10^{3}$	$27.86*10^{3}$	$37.83*10^{3}$
Mass (kg)	$2.32*10^{-1}$	$1.30*10^{-1}$	$1.05*10^{-1}$	$0.68*10^{-1}$
TMR (N.m/kg)	$46.55*10^{-1}$	$36.92*10^{-1}$	$38.38*10^{-1}$	$58.68*10^{-1}$
Power consumption (W)	8.00	6.25	5.20	-
TPR (N.m/W)	$13.50*10^{-2}$	$7.68*10^{-2}$	$7.75*10^{-2}$	-

[a] MR brake includes 28:120 gear train.
[b] Saturation torque

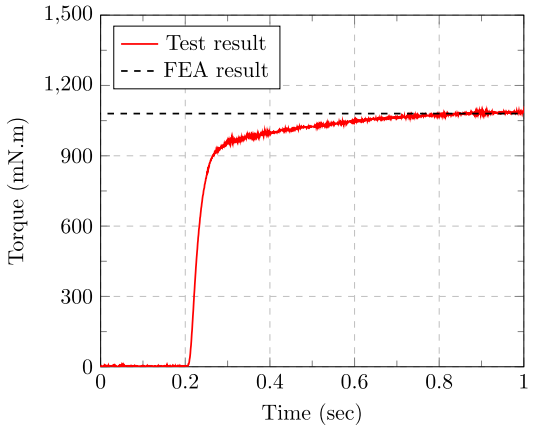

FIGURE 15. Results of test and FEA under a step current of 860 mA.

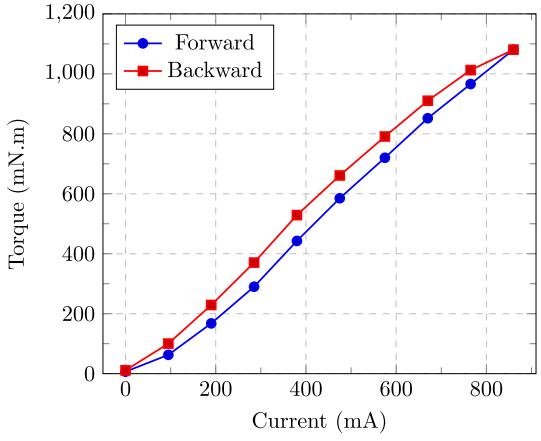

FIGURE 16. Relationship between output torque and input current.

In the experiment, a step current of 860 mA was applied, then, the torque of about 1080 mN.m was observed (see FIGURE 15). In addition, a series of currents between 0 and 860 mA were also applied. The current was increased from 0 mA with a step of about 95 mA. After reaching 860 mA, the current was reduced to 0 mA with the same step. The relationship between the output torque and the input current is shown in FIGURE 16. The viscous torque was observed to be about 11 mN.m.

As shown in TABLE 3, FEA had a good estimate on the saturation torque. Hence, the simulated TVR was very close to the actual TVR. Due to the fact that the brake assembly included some screws and fasteners, the actual mass of the brake was slightly larger than the simulated mass, resulting in a slightly smaller actual TMR than the simulated value. The actual power consumption was also slightly larger than the simulated value, resulting in a slightly smaller actual TPR than the simulated value. The reason might be that the winding efficiency in FEA simulation was not accurate enough. Generally, the FEA results were consistent with the actual test results.

The performance comparisons among the small-scale MR brakes with different architectures are displayed in TABLE 4. The fabricated brake had larger TVR than the other three MR brakes. Both TMR and TPR of the fabricated brake were larger than those of the multi-disk and the multi-drum brakes. But TMR of the fabricated brake was smaller than that of the drum brake.

V. CONCLUSION

This paper focuses on a hollowed multi-drum MR brake which has a hollow casing and several drum-like rotors and stators and evaluates the influence of the hollow casing radius on the performance of this type of MR brake. The brakes with different hollow casing radii were optimized via FEA to ensure that the flux density over the smallest gap was around the MRF-122EG saturation point and the maximal flux density along the iron flux path was around the DT4C saturation point. After obtaining all optimal designs, the torque, volume, mass, and power consumption including TVR, TMR, and TPR were calculated and evaluated. The results indicated that the overall performance of the brake improved with the increase of the hollow casing radius. In order to verify FEA, the brake with 8 mm hollow casing radius was fabricated, assembled and tested. The test results showed that FEA had a good estimate on saturation torque. The actual TVR was very close to the simulated value. The actual mass and power consumption were slightly larger than the simulated values, resulting in the slight smaller actual TMR and TPR than the simulated values. Generally, the FEA results were consistent with the actual test results. The results of this paper showed that the hollow casing radius should be kept as large as possible within the design range in a hollowed multi-drum

MR brake design. The designers should also pay attention to TVR and TMR since their increasing trends were limited after about 100 mm radius.

REFERENCES

[1] J. D. Carlson, "What makes a good mr fluid?" *J. Intell. Mater. Syst. Struct.*, vol. 13, nos. 7–8, pp. 431–435, 2002.
[2] J. Blake and H. B. Gurocak, "Haptic glove with MR brakes for virtual reality," *IEEE/ASME Trans. Mechatronics*, vol. 14, no. 5, pp. 606–615, Oct. 2009.
[3] H. Qin, A. Song, Z. Gao, Y. Liu, and G. Jiang, "A multi-finger interface with mr actuators for haptic applications," *IEEE Trans. Haptics*, vol. 11, no. 1, pp. 5–14, Jan./Mar. 2018.
[4] F. Gao, Y.-N. Liu, and W.-H. Liao, "Optimal design of a magnetorheological damper used in smart prosthetic knees," *Smart Mater. Struct.*, vol. 26, no. 3, 2017, Art. no. 035034.
[5] R. M. Andrade, A. B. Filho, C. B. S. Vimieiro, and M. Pinotti, "Optimal design and torque control of an active magnetorheological prosthetic knee," *Smart Mater. Struct.*, vol. 27, no. 10, 2018, Art. no. 105031.
[6] E. J. Park, D. Stoikov, L. F. da Luz, and A. Suleman, "A performance evaluation of an automotive magnetorheological brake design with a sliding mode controller," *Mechatronics*, vol. 16, no. 7, pp. 405–416, 2006.
[7] K. Karakoc, E. J. Park, and A. Suleman, "Design considerations for an automotive magnetorheological brake," *Mechatronics*, vol. 18, no. 8, pp. 434–447, 2008.
[8] Q. H. Nguyen and S. B. Choi, "Optimal design of an automotive magnetorheological brake considering geometric dimensions and zero-field friction heat," *Smart Mater. Struct.*, vol. 19, no. 11, 2010, Art. no. 115024.
[9] H. Guo and W.-H. Liao, "Optimization of a multifunctional actuator utilizing magnetorheological fluids," in *Proc. IEEE/ASME Int. Conf. Adv. Intell. Mechatronics (AIM)*, Jul. 2011, pp. 67–72.
[10] Q. H. Nguyen and S. B. Choi, "Selection of magnetorheological brake types via optimal design considering maximum torque and constrained volume," *Smart Mater. Struct.*, vol. 21, no. 1, 2011, Art. no. 015012.
[11] W. Li, P. Yadmellat, and M. R. Kermani, "Design optimization and comparison of magneto-rheological actuators," in *Proc. IEEE Int. Conf. Robot. Automat. (ICRA)*, May/Jun. 2014, pp. 5050–5055.
[12] H. Ma, B. Chen, L. Qin, and W.-H. Liao, "Design and testing of a regenerative magnetorheological actuator for assistive knee braces," *Smart Mater. Struct.*, vol. 26, no. 3, 2017, Art. no. 035013.
[13] S. R. Patil, K. P. Powar, and S. M. Sawant, "Thermal analysis of magnetorheological brake for automotive application," *Appl. Therm. Eng.*, vol. 98, pp. 238–245, Apr. 2016.
[14] J. Yu, X. Dong, P. Chen, A. Rakhio, and A. A. Laghari, "Optimal design methodology of magneto-rheological (MR) rotary brake for robotic ankle systems considering temperature effects," in *Proc. 2nd Int. Conf. Robot. Artif. Intell. (ICRAI)*, Nov. 2016, pp. 180–185.
[15] H. Shamieh and R. Sedaghati, "Development, optimization, and control of a novel magnetorheological brake with no zero-field viscous torque for automotive applications," *J. Intell. Mater. Syst. Struct.*, vol. 29, no. 16, pp. 3199–3213, 2018.
[16] P. Fauteux, M. Lauria, M.-A. Legault, B. Heintz, and F. Michaud, "Dual differential rheological actuator for robotic interaction tasks," in *Proc. IEEE/ASME Int. Conf. Adv. Intell. Mechatronics*, Jul. 2009, pp. 47–52.
[17] K. H. Gudmundsson, F. Jonsdottir, and F. Thorsteinsson, "A geometrical optimization of a magneto-rheological rotary brake in a prosthetic knee," *Smart Mater. Struct.*, vol. 19, no. 3, 2010, Art. no. 035023.
[18] D. Senkal and H. Gurocak, "Serpentine flux path for high torque MRF brakes in haptics applications," *Mechatronics*, vol. 20, no. 3, pp. 377–383, 2010.
[19] B. Gonenc and H. Gurocak, "Virtual needle insertion with haptic feedback using a hybrid actuator with DC servomotor and MR-brake with Hall-effect sensor," *Mechatronics*, vol. 22, no. 8, pp. 1161–1176, 2012.
[20] M. Avraam, M. Horodinca, I. Romanescu, and A. Preumont, "Computer controlled rotational mr-brake for wrist rehabilitation device," *J. Intell. Mater. Syst. Struct.*, vol. 21, no. 15, pp. 1543–1557, 2010.
[21] N. Q. Hung and C. S. Bok, "Optimal design of a T-shaped drum-type brake for motorcycle utilizing magnetorheological fluid," *Mech. Based Des. Struct. Mach.*, vol. 40, no. 2, pp. 153–162, 2012.
[22] R. Demersseman, M. Hafez, B. Lemaire-Semail, and S. Clénet, "Magnetorheological brake for haptic rendering," in *Proc. Int. Conf. Hum. Haptic Sens. Touch Enabled Comput. Appl.* Berlin, Germany: Springer, 2008, pp. 941–945.
[23] D. Senkal and H. Gurocak, "Spherical brake with mr fluid as multi degree of freedom actuator for haptics," *J. Intell. Mater. Syst. Struct.*, vol. 20, no. 18, pp. 2149–2160, 2009.
[24] Y. Shiao, N. A. Ngoc, and C.-H. Lai, "Optimal design of a new multipole bilayer magnetorheological brake," *Smart Mater. Struct.*, vol. 25, no. 11, 2016, Art. no. 115015.
[25] H. Qin, A. Song, X. Zeng, and S. Hu, "Design and evaluation of a small-scale multi-drum magnetorheological brake," *J. Intell. Mater. Syst. Struct.*, vol. 29, no. 12, pp. 2607–2618, 2018.

HUANHUAN QIN was born in Ma'anshan, China, in 1989. He received the B.S. degree in measurement and control technology and instrumentation from Anhui Polytechnic University, Wuhu, China, in 2012. He is currently pursuing the Ph.D. degree with the School of Instrument Science and Engineering, Southeast University, Nanjing, China.

His current research interests include haptic display, haptic devices, and magnetorheological actuators.

AIGUO SONG (M'98–SM'12) was born in Huangshan, China, in 1968. He received the B.S. degree in automatic control and the M.S. degree in measurement and control from the Nanjing University of Aeronautics and Astronautics, Nanjing, China, in 1990 and 1993, respectively, and the Ph.D. degree in measurement and control from Southeast University, Nanjing, China, in 1996.

From 1996 to 1998, he was an Associate Researcher with the Intelligent Information Processing Laboratory, Southeast University, where he was an Associate Professor with the Department of Instrument Science and Engineering, from 1998 to 2000, and the Director of the Robot Sensor and Control Laboratory, from 2000 to 2003. From April 2003 to April 2004, he was a Visiting Scientist with the Laboratory for Intelligent Mechanical Systems, Northwestern University, Evanston, IL, USA. He is currently a Professor with the School of Instrument Science and Engineering, Southeast University. His current research interests include teleoperation, haptic display, the Internet telerobotics, and distributed measurement systems.

YITING MO was born in Yiyang, China, in 1996. She received the B.S. degree in measurement and control technology and instrumentation from the Nanjing University of Aeronautics and Astronautics, Nanjing, China, in 2017. She is currently pursuing the Ph.D. degree with the School of Instrument Science and Engineering, Southeast University, Nanjing, China. Her research interests include magnetorheological actuators and wearable haptic devices.